

stirred at 25 °C for 7 h under nitrogen. After evaporation of the solvent in vacuo (<30 °C), the residue was dissolved in methanol and chromatographed on preparative silica gel plates (1-propanol/10% aqueous NH₃, 95/5 v/v) to give the model compound **3**: yield 113.3 mg (0.57 mmol; 93.6%); MS (70 eV, $T_d = 100$ °C) 152 (100), 194 (65), 195 (7), 196 (3) (M⁺); UV (MeOH) λ_{max} 270 (ϵ 5.92 × 10⁶ cm²/mol), 310 nm (ϵ 3.07 × 10⁶ cm²/mol); ¹H NMR (250 MHz, CD₃OD) δ 3.4 (1 H), 3.53 (t, $J = 8.2$ Hz, 2 H), 3.65 (s, 3 H), 4.39 (t, $J = 8.2$ Hz, 2 H), 6.6 (d, 1 H), 7.96 (dd, 1 H), 8.25 (d, 1 H); ³J₅₆ = 9.1 Hz, ⁴J₂₆ = 3.3 Hz; ¹³C NMR (62.9 MHz, CD₃OD) δ 34.43 (t, CH₂-S), 38.39 (q, CH₃N), 63.85 (t, CH₂N), 70.09 (d, C-4), 114.29 (s, C-3), 120.1 (d, C-5), 139.66 (d, C-6), 143.44 (d, C-2), 164.75 (s, CONH), 169.43 (s).

Preparation of Samples for NMR Measurements. Two series of experiments for the NAD binding studies were carried out with slightly different enzyme concentrations. In the following, data for series 2 are in parentheses. To 45.12 (32.69) mg of GAPDH in 1.6 mL of buffer solution (1 mM potassium phosphate, pH 7.0, 0.5 mM EDTA, and 0.5 mM dithiothreitol) was added 0.2 mL of ²H₂O, resulting in a final concentration of 0.174 (0.126) mM for the tetrameric enzyme.

The [4-¹³C]NAD solutions used in the two series of experiments also differed slightly (see Table II). The two solutions contained 2.41 (1.05) mg of β -NAD in 0.173 (0.100) mL of the above buffer. Introduction of a 10- μ L aliquot of this coenzyme solution into the enzyme sample resulted in the addition of 0.68 (0.70) equiv of β -NAD to the tetrameric GAPDH.

Determination of Enzyme and Coenzyme Concentrations. Since NMR monitoring of the binding of β -NAD to GAPDH disclosed unexpected behavior, precise determination of concentrations was required. The enzyme concentration was determined by enzymic assay²⁷ on the one hand and by measuring the protein concentration on the other. The latter was determined by the Warburg method, which was specially adapted for GAPDH by Seydoux et al.³ Protein determinations at the Karlsruhe and Strasbourg laboratories using this method did not differ by more than 2%. Two different methods were also applied for the determination of coenzyme concentrations, and after correction for the amounts of α -NAD and NMN present, they gave consistent results. The percentages of the different nicotinamide nucleotide species in the coenzyme samples were determined by ¹³C NMR and independently by HPLC.²⁸

After each addition of [4-¹³C]NAD a 20- μ L aliquot of the mixture was withdrawn, and its NAD content was determined according to the method of Seydoux et al.³ Since this method relies on the UV absorption at 260 nm, the determination also includes unbound α -NAD. Taking this into account, the calculated β -NAD values showed good agreement with those determined independently by the yeast alcohol dehydrogenase reaction (Table II).²⁹ Variations of the enzyme concentration in the

reaction mixture caused by withdrawal and/or addition of aliquots are also accounted for in the tables.

¹³C NMR Spectroscopy. ¹³C NMR spectra of the enzyme/coenzyme mixtures were obtained at 125.7 MHz (11.7 T) on a Bruker AM-500 FT-NMR spectrometer. The ca. 1.8-mL samples were measured at a controlled temperature of 15 °C in 10-mm sample tubes (nonspinning without a vortex plug to avoid a Teflon background signal). Chemical shifts were referenced to internal dioxane ($\delta_c = 67.8$ ppm) by use of a separate buffer solution. All measurements were performed with the standard inverse-gated decoupling technique to obtain ¹H-decoupled spectra with suppression of the nuclear Overhauser effect (NOE) in order to ensure that signal integrals were proportional to concentrations for all species. Parameters for data acquisition were spectral width = 33 kHz for 16K time domain points with an acquisition time of 0.246 s and pulse width = 15 μ s (flip angle ca. 60°). The relaxation delay with the decoupler turned off was 0.6 s for spectra 1.1–1.7 of series 1 and 1.6 s for spectra 1.7b, 1.8, and 1.9 and spectra of series 2. Comparing spectra 1.7 and 1.7b acquired for the same sample showed that a relaxation delay of 0.6 instead of 1.6 s led to an increase in the integrals for the nonbinding species α -NAD and NMN (partial NOE) but had no effect on bound or free β -NAD. Increasing the delay to 2.3 s (spectrum 1.9b) caused no further change in any signal intensities. Therefore, the spectra of series 2 were all obtained with the 1.6-s delay. For spectra 1.1–1.7 the integrals measured for α -NAD and NMN were corrected for the observed effect of the shorter delay. The number of transients acquired for each spectrum ranged from 4000 (spectra 1.8 and 1.9 in 2 h) to 40000 (spectrum 2.5 in 20 h).

Spectra were Fourier transformed with 32K data points (a) after an exponential multiplication with 30-Hz line broadening for quantitative analysis of total free and total bound species (Figure 2) and (b) with a Lorentz-Gauss resolution enhancement (Bruker software; LB = -8; GB = 0.1) for separate integration and line-width evaluation of the resolved signals for free β -NAD, α -NAD, and NMN (Figures 3 and 6). Transforms were in absolute-intensity mode referenced to spectrum 1.7b, and integrals were then appropriately scaled according to the different number of transients acquired for each spectrum to give the data of Table I and Figure 4. The integrals from the spectra of series 2 were also corrected by a scaling factor which took into account the lower initial enzyme concentration compared to that in series 1. The scaling factors used were also applied to the spectra themselves to produce the figures. Subtraction of spectrum 1.7 or 1.7b from individual scaled spectra obtained with the same relaxation delay showed that the theoretical scaling factors agreed with empirical scaling factors within ca. 5%, as judged by cancellation of the lysine signal of GAPDH at ca. 40 ppm. Integration of the base line corrected spectra was performed digitally with the standard routines of the Bruker NMR software.

Acknowledgment. We thank P. Barth for help in the enzyme purification and the Deutsche Forschungsgemeinschaft and the Fonds der Chemischen Industrie for financial support. J.K. thanks the province of Baden-Württemberg for a scholarship.

- (27) Ferdinand, W. *Biochem. J.* **1964**, *92*, 578–585.
 (28) Richard, A. H.; Sebastian, P. A.; Phyllis, R. B. *J. Chromatogr.* **1979**, *186*, 647–658.
 (29) Lowry, O. H.; Passonneau, J. V. *A Flexible System of Enzymatic Analysis*; Academic Press: New York, 1972.

Hydrolysis of *N*-Acetyl-*p*-benzoquinone Imines: pH Dependence of the Partitioning of a Tetrahedral Intermediate

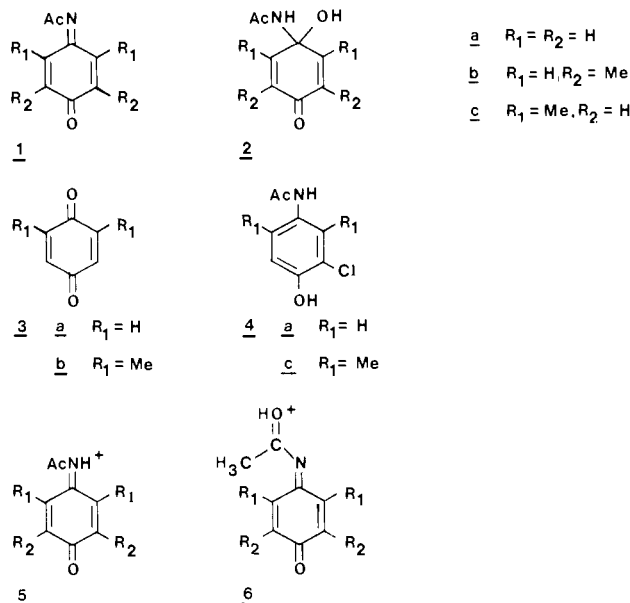
Michael Novak,* Gayl A. Bonham, Julio J. Mulero,^{1a} Maria Pelecanou,^{1a} Joseph N. Zemis,^{1a} Jeanne M. Buccigross,^{1b} and Thomas C. Wilson

Contribution from the Department of Chemistry, Miami University, Oxford, Ohio 45056.
 Received November 17, 1988

Abstract: The hydrolysis reactions of *N*-acetyl-*p*-benzoquinone imine, **1a**, and its 3,5- and 2,6-dimethyl analogues, **1b** and **1c**, in the pH range 0.3–10.5 are described. At pH < 6.0 the carbinolamide intermediates **2a–c** can be detected by ¹H NMR, UV, and HPLC methods. The pH-dependent partitioning of **2a** and **2c** can be monitored since the reversion of these intermediates to the protonated *N*-acylimines **5a** and **5c** leads to products of the conjugate attack of Cl⁻, the 3-chloroacetaminophen derivatives **4a** and **4c**. A mechanism for the hydrolysis of **1a–c** (Scheme I) is proposed which accurately predicts the time dependence of the formation of **2** and the final hydrolysis products, the *p*-benzoquinones **3**, and **4**. The alternative O-protonation mechanism (Scheme II) is tentatively rejected on the basis of substituent effect data. The relationship of the hydrolysis reactions of **1a–c** to those of ordinary imines is discussed.

N-Acetyl-*p*-benzoquinone imine (**1a**) is an apparent toxic metabolite of the common analgesics acetaminophen and phen-

acetin.² The mechanism of action of **1** in vivo is not well understood, and little is known of its aqueous-solution chemistry.



We previously reported that the kinetics of hydrolysis of **1a** are characterized by two consecutive first-order processes at pH < 6.0.³ The tetrahedral intermediate **2a** was detected and characterized by NMR, UV, and HPLC methods.^{3a} The disappearance of **1a** is acid catalyzed in this pH region, and **2a** decomposes by acid-dependent, neutral, and base-dependent paths,³ but the detailed mechanism of hydrolysis of **1a** was not addressed.

In this paper, we present results of a study of the hydrolysis of **1a** and its dimethyl analogues *N*-acetyl-3,5-dimethyl-*p*-benzoquinone imine (**1b**) and *N*-acetyl-2,6-dimethyl-*p*-benzoquinone imine (**1c**) in the pH range 0.3–10.5. In all three cases, the disappearance of **1** involves acid-dependent, neutral, and base-dependent paths. Kinetic data obtained by UV and HPLC methods allow a description of the pH-dependent partitioning of **2a** or **2c** between the product quinones **3a** or **3b**, the starting *N*-acetylquinone imines **1a** or **1c**, and the 3-chloro products **4a** or **4c**, which are formed by conjugate attack of Cl⁻ on protonated **1a** or **1c**.

A hydrolysis mechanism consistent with kinetic and product data, substituent effects, and solvent isotope effects has been proposed, and kinetic simulations show that the mechanism accurately predicts the time dependence of the evolution of **2–4** as determined by HPLC experiments. The effect of the dimethyl substituents on the rate of the acid-catalyzed hydrolysis of **1c** appears to favor a mechanism involving the N-protonated intermediate **5**, rather than the kinetically indistinguishable path involving the O-protonated species **6**.

The hydrolysis reactions of **1** differ in many respects from most reactions involving the interconversion of imine and carbonyl groups in aqueous solution.^{4,5} These differences and the reasons behind them are discussed herein.

Experimental Section

Synthesis. The *N*-acetylquinone imines **1a–c** were synthesized by literature methods^{6,7} and purified by sublimation at reduced pressure. Spectral and physical data were consistent with those previously reported.^{3,6,7} Authentic **4a** was available from a previous study,⁸ and **4c**, 3-chloro-4-hydroxy-2,6-dimethylacetanilide, was synthesized as described in the literature.⁷ The quinone **3b** was prepared by oxidation of 2,6-dimethylhydroquinone with freshly prepared Ag₂O⁹ and purified by sublimation at reduced pressure. Physical and spectral data for **3b** were consistent with the structure and previously reported data.¹⁰

The quinols **8a–c** were synthesized from **3a** and **3b** by literature procedures.^{11,12} These materials were purified by sublimation followed by recrystallization from hexanes (**8a**, **8c**) or *n*-pentane (**8b**). Physical and spectral data were consistent with the structures and with previously published data.¹³

Kinetic Measurements. Kinetics were performed in 5 vol % CH₃CN–H₂O solutions or CD₃CN–D₂O solutions. General procedures for UV absorption spectroscopy and HPLC methods have been described.^{8,14} Kinetic measurements were performed at 25.0 ± 0.1 °C in HCl solutions and in formate, acetate, phosphate, or borate buffers (0.01–0.20 M). All solutions were maintained at 0.5 M ionic strength with KCl or KCl–KClO₃. All pH readings were taken at 25.0 ± 0.1 °C with an Orion Model 701A digital pH meter equipped with a Radiometer GK 2402C combination electrode. Measurements of pH or pD on standardized HCl or DCl solutions in the range 0.001–0.1 M established the following relationships between pH or pD and the meter reading:

$$\text{pH} = \text{meter reading} - 0.05 \quad (1)$$

$$\text{pD} = \text{meter reading} + 0.35 \quad (2)$$

Values for $\text{p}K_w$ of 13.95 and 14.82 were established in H₂O and D₂O, respectively, by pH measurements on standardized solutions of KOH (KOD) in the concentration range 0.005–0.05 M.

Kinetic measurements were performed by UV and HPLC methods as described previously for **1a**.³ Concentrations of **1** used in the UV study were either ca. 5 × 10⁻⁵ or ca. 2.5 × 10⁻⁶ M. In the HPLC studies concentrations of **1** of ca. 1.0 × 10⁻⁴ M were ordinarily used. Wavelengths monitored in the UV study were as follows: for **1a**, 266.5 and 245 nm at pH < 6.5, and 261.8 and 225.8 nm at pH > 6.5; for **1b**, 275.3 and 255.8 nm at pH < 7.5, and 275 nm at pH > 7.5; for **1c**, 276 and 256 nm at pH < 7.5, and 275 nm at pH > 7.5. The wavelengths at higher pH were chosen to correspond to isobestic points for the base-induced hydrolysis of the quinones **3a** and **3b**. In the HPLC study, the UV detector was set at 225 or 250 nm. Absorbance vs time, or peak area vs time data were fit by nonlinear least-squares procedures^{8,14} to either the standard first-order rate equation (three-parameter fit) or to the equation for consecutive first-order processes (eq 3) (five-parameter fit). The

$$A_t = A_1 \exp(-k_1 t) + A_2 \exp(-k_2 t) + A_\infty \quad (3)$$

quality of these fits, as judged by agreement between observed and calculated A_0 and A_∞ values and the standard deviations of the fits, was excellent. Kinetic simulations were performed with the MIREAK¹⁵ software on an IBM XT equipped with 640K bytes of RAM and an 8087 math coprocessor.

Product Analyses. Product studies were performed at the end of the kinetic runs by triplicate HPLC injections. The averaged peak areas were converted to concentrations by calibration with known concentrations of the authentic products **3a**, **3b**, **4a**, and **4c**. Details of the method have been published.^{3,8,14} Identities of **3a** and **3b** were established by HPLC coinjection of authentic samples and from NMR of reaction mixtures run

(1) (a) Department of Chemistry, Clark University, Worcester, MA 01610. (b) Department of Chemistry, College of Mount St. Joseph, Mount St. Joseph, OH 45051.

(2) Dahlin, D. C.; Miwa, G. T.; Lu, A. Y. H.; Nelson, S. D. *Proc. Natl. Acad. Sci. U.S.A.* **1984**, *81*, 1327–1331. Corcoran, G. B.; Mitchell, J. R.; Vaishnav, Y. N.; Horning, E. C. *Molec. Pharmacol.* **1980**, *18*, 536–542. Mulder, G. J.; Hinson, J. A.; Gillette, J. R. *Biochem. Pharmacol.* **1978**, *27*, 1641–1647. Potter, D. W.; Hinson, J. A. *J. Biol. Chem.* **1987**, *262*, 966–973.

(3) (a) Novak, M.; Pelecanou, M.; Pollack, L. *J. Am. Chem. Soc.* **1986**, *108*, 112–120. (b) Novak, M.; Pelecanou, M.; Zemis, J. N. *J. Med. Chem.* **1986**, *29*, 1424–1429.

(4) (a) Cordes, E. H.; Jencks, W. P. *J. Am. Chem. Soc.* **1962**, *84*, 832–837. (b) Cordes, E. H.; Jencks, W. P. *J. Am. Chem. Soc.* **1963**, *85*, 2843–2848. (c) Kayser, R. H.; Pollack, R. M. *J. Am. Chem. Soc.* **1977**, *99*, 3379–3387. (d) Sayer, J. M.; Conlon, P. J. *J. Am. Chem. Soc.* **1980**, *102*, 3592–3600. (e) Okuyama, T.; Shibuya, H.; Fueno, T. *J. Am. Chem. Soc.* **1982**, *104*, 730–736. (f) Corbett, J. F. *J. Chem. Soc. B* **1969**, 213–216.

(5) Rosenberg, S.; Silver, S. M.; Sayer, J. M.; Jencks, W. P. *J. Am. Chem. Soc.* **1974**, *96*, 7986–7997. Sayer, J. M.; Pinsky, B.; Schonbrunn, A.; Washtein, W. *J. Am. Chem. Soc.* **1974**, *96*, 7998–8009.

(6) Dahlin, D. C.; Nelson, S. D. *J. Med. Chem.* **1982**, *25*, 885–886.

(7) Fernando, C. R.; Calder, I. C.; Ham, K. N. *J. Med. Chem.* **1980**, *23*, 1153–1158.

(8) Novak, M.; Pelecanou, M.; Roy, A. K.; Andronico, A. F.; Plourde, F. M.; Olefirowicz, T. M.; Curtin, T. J. *J. Am. Chem. Soc.* **1984**, *106*, 5623–5631.

(9) Fieser, L. F.; Fieser, M. *Reagents for Organic Synthesis*; Wiley: New York, 1967; Vol. 1, p 1011.

(10) Nolting, E.; Bauman, T. *Chem. Ber.* **1985**, *118*, 1150–1152.

(11) Fischer, A.; Henderson, G. N. *Tetrahedron Lett.* **1980**, *21*, 701–704.

(12) Liotta, D.; Saindane, M.; Barnum, C. *J. Org. Chem.* **1981**, *46*, 3369–3370.

(13) Bamberger, E. *Chem. Ber.* **1903**, *36*, 2028–2042. Adler, E.; Dahlen, J.; Westin, G. *Acta Chem. Scand.* **1960**, *14*, 1580–1596. Omura, Y.; Nakamura, M. Japanese Patent 74/127937, 1974; *Chem. Abstr.* **1975**, *82*, 170383.

(14) Novak, M.; Roy, A. K. *J. Org. Chem.* **1985**, *50*, 571–580.

(15) Copyright 1984, Kenneth A. Wilde, 3604 Laurel Ledge Lane, Austin, TX 78731.

Table IV. Rate Constants Derived from Eq 5 and 6^a

<i>N</i> -acetylquinone imine	k_H' , M ⁻¹ s ⁻¹	$10^5 k_c'$, s ⁻¹	k_{OH}' , M ⁻¹ s ⁻¹	$10^2 k_H''$, M ⁻¹ s ⁻¹	$10^4 k_c''$, s ⁻¹	$10^{-5} k_{OH}''$, M ⁻¹ s ⁻¹
1a	145 ± 5 (0.39 ± 0.02)	1.89 ± 0.11 (1.69 ± 0.12)	13.7 ± 0.9 (0.52 ± 0.04)	5.72 ± 0.22 (0.39 ± 0.02)	4.26 ± 0.04 (1.18 ± 0.01)	4.50 ± 0.27 (0.55 ± 0.04)
1b	311 ± 21 (0.43 ± 0.03)	0.269 ± 0.050 (1.64 ± 0.36)	1.92 ± 0.23 (0.61 ± 0.08)	35.3 ± 0.7 (0.42 ± 0.01)	8.11 ± 0.04 (1.24 ± 0.01)	5.65 ± 0.19 (0.58 ± 0.03)
1c	0.0156 ± 0.0003 (0.40 ± 0.01)	1.63 ± 0.01 (2.01 ± 0.01)	3.70 ± 0.08 (0.70 ± 0.03)	0.0521 ± 0.0050 (0.75 ± 0.11)	13.2 ± 0.1 (1.26 ± 0.02)	4.76 ± 0.98 (0.30 ± 0.12)

^a Solvent isotope effects (k_{H_2O}/k_{D_2O}) for each parameter are shown in parentheses.

in D₂O. The anilides **4a** and **4c** were identified by isolation⁸ and comparison to authentic samples.

NMR Studies. The decomposition of **1b** and **1c** was monitored by NMR at either 250 MHz or 90 MHz as previously described for **1a**.^{3a} ¹H NMR spectra were recorded in 0.001 N DCl solutions at 5 °C for **1b** and in 0.1 N DCl at ambient temperature for **1c**. DSS was used as an internal standard.

pK_a Measurements. The pK_a of **8a–c** were determined in 5% CH₃CN–H₂O (μ = 0.5 M KCl) by spectrophotometric titration or titrimetric methods. In the spectrophotometric method, absorbance vs pH data (at 228 nm for **8a**, 238 nm for **8b**) obtained from 5.0 × 10⁻⁵ M solutions of **8a** or **8b** in KOH solutions in the pH range 11.6–13.9 were fit to eq 4

$$A_T = A_{AH} \left[\frac{[H^+]}{K_a + [H^+]} \right] + A_{A^-} \left[\frac{K_a}{K_a + [H^+]} \right] \quad (4)$$

by a nonlinear least-squares procedure in which A_{AH} , A_{A^-} , and K_a were treated as variable parameters. Total absorbance changes were ca. 0.08 AU and the standard deviations of the fits were less than 0.001 AU.

In the titrimetric method, the consumption of OH⁻ by addition of 0.05 M quinol was monitored with the pH electrode in KOH solutions ranging from 0.01 to 0.1 M. The value of K_a could then be calculated from K_w , the concentration of quinol, and the known consumption of OH⁻. Values of pK_a were reproducible within ±0.1 and were in good agreement with those determined spectrophotometrically.

MNDO Calculations. The version of MNDO¹⁶ used here is that found in MOPAC 4.0.¹⁷ Calculations were performed on an IBM 4381 Model 23 running under VM/CMS. The geometries of **1a**, **5a**, **6a**, **5c**, and **6c** were optimized with respect to all geometrical parameters with the Broyden–Fletcher–Goldfarb–Shanno algorithm incorporated into MOPAC. Gradients were routinely reduced to <0.4 kcal mol⁻¹ Å⁻¹ or kcal mol⁻¹ radian⁻¹.

Results

Kinetics and Products. The kinetics of hydrolysis of **1a–c** were monitored by UV methods at 25 °C in 5 vol % CH₃CN–H₂O or CD₃CN–D₂O at 0.5 M ionic strength in the pH region 0.3–10.5. Throughout this pH region, **1b** and **1c** exhibited clean pseudo-first-order or consecutive first-order hydrolysis kinetics. At pH > 6.5 reduction to acetaminophen and subsequent oligomerization reactions involving **1a** and acetaminophen competed with the hydrolysis unless the buffers contained 0.05 M KClO₃ and the initial concentration of **1a** was reduced from 5.0 × 10⁻⁵ to ca. 2.5 × 10⁻⁶ M. Under these conditions, first-order kinetics were obtained and HPLC analysis showed that reduction of **1a** accounted for less than 10% of the overall reaction. In the absence of KClO₃ and at initial concentrations of 1.0 × 10⁻⁴ M, HPLC analysis of reaction mixtures showed that **1c** underwent no detectable reduction and less than 2% of the reduction product (3,5-dimethylacetaminophen) was detected in hydrolysis mixtures of **1b**.

As previously described for **1a**,³ the absorbance vs time data for **1a–c** could be fit to either the first-order rate equation or eq 3. Absorbance data taken at 266.5 nm for **1a**, 275.3 nm for **1b**, and 275 nm for **1c** under acidic and neutral conditions and at the isosbestic points for hydrolysis of the product quinones **3a** or **3b** under basic conditions (see the Experimental Section), were fit by the first-order rate equation to yield a pH-dependent rate constant, k' , which is reported in Tables I–III in the microfilm edition (see the supplementary material). Previously published data,^{3a} and rate constants reported in Tables I–III show that although k' is pH dependent, it is insensitive to buffer concen-

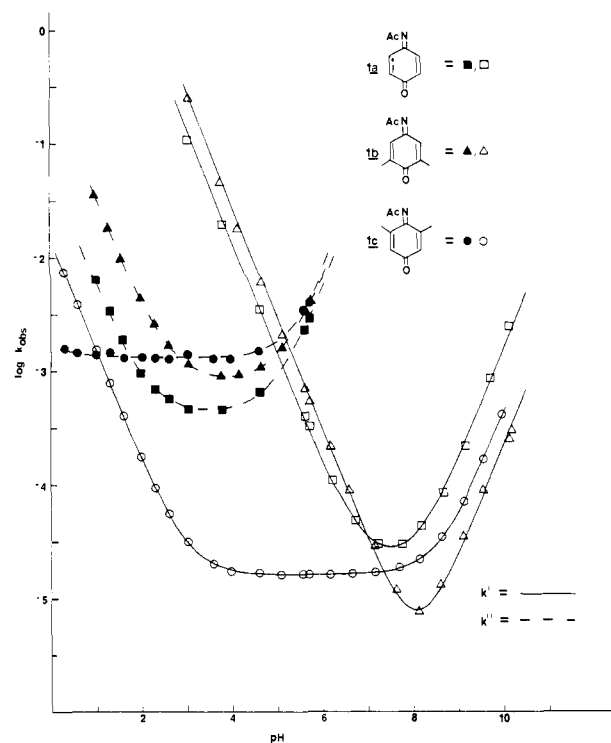


Figure 1. pH-rate profiles for the hydrolysis of **1a–c** at 25 °C in 5 vol % CH₃CN–H₂O (μ = 0.5 M). Theoretical lines for k' and k'' were obtained by least-squares fits of the data to eq 5 and 6.

tration. At pH < 5.0 kinetic measurements for **1a** and **1c** were confined to the buffer concentration range 0.01–0.05 M because the rate of disappearance of these two species depends on [Cl⁻] (see below) under acidic conditions. Chloride is present to maintain ionic strength and its concentration decreases considerably in more concentrated buffers. Since [Cl⁻] has no effect on the reactions of **1b** (see below), the disappearance of **1b** was monitored in buffers ranging from 0.01–0.20 M under acidic conditions. The pH dependence of k' is described by eq 5. The

$$k' = k_H'[H^+] + k_c' + k_{OH}'[OH^-] \quad (5)$$

rate constants derived from a weighted least-squares fit of the rate data to eq 5 are reported in Table IV with values of the solvent isotope effect (k_{H_2O}/k_{D_2O}). The quality of the fit of the rate data to eq 5 is evident in Figure 1.

At pH < 6.0,¹⁸ absorbance data taken at 245 nm for **1a** and at 255.8 nm for **1b** and **1c** were fit by eq 3 to yield two rate constants, one of which is experimentally equivalent to k' . The other, k'' , is also pH dependent, but it is insensitive to buffer concentration (Tables I–III). The results of weighted least-squares fits of k'' to eq 6 are presented in Table IV and Figure 1.

$$k'' = k_H''[H^+] + k_c'' + k_{OH}''[OH^-] \quad (6)$$

The behavior shown in Figure 1 requires the existence of a detectable intermediate, which we previously identified as **2a** in the case of **1a**.^{3a} ¹H NMR spectra taken during the hydrolysis

(16) Dewar, M. J. S.; Thiel, W. J. *Am. Chem. Soc.* **1977**, *99*, 4899–4906, 4907–4917.

(17) Quantum Chemistry Program Exchange, QCPE 455.

(18) The k'' process can be observed in most cases up to pH = 6.5, but the small absorbance changes at pH > 6.0 make it difficult to obtain accurate rate constants.

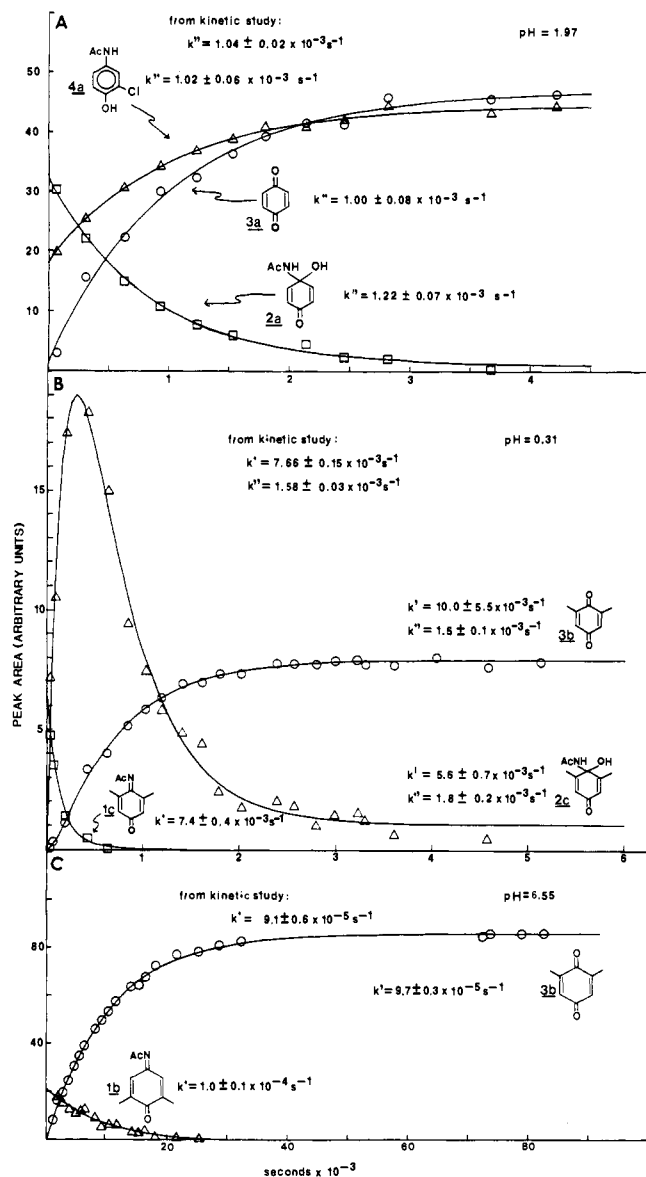


Figure 2. Plots of HPLC peak areas vs time obtained during the hydrolysis of **1a-c**. Rate constants and theoretical lines were determined by a least-squares fit of the data to the first-order rate equation, or to eq 3: (A) data obtained for **1a** at pH 1.97, (B) data obtained for **1c** at pH 0.31, and (C) data obtained for **1b** at pH 6.55.

of **1b** and **1c** also provide evidence for structures **2b** and **2c**. In 10^{-3} M DCl at 5°C , **1b** cannot be detected by NMR within 1 min of mixing, but an intermediate which decomposes, with a half-life of 1.1 h, into **3b** and acetamide (confirmed by NMR of authentic samples), can be readily observed. The spectrum [(250 MHz, D_2O) δ 1.86 (6 H, s), 1.96 (3 H, s), 6.86 (2 H, s)] is consistent with **2b**, as is the identity of its decomposition products. The decomposition of **1c** is much slower under acidic conditions (see Table IV and Figure 1), so it can be readily observed at early reaction times of 0.1 N DCl at ambient temperature [(90 MHz, D_2O) δ 2.09 (6 H, s, br), 2.44 (3 H, s), 6.53 (2 H, s)]. This material quickly decomposes into **2c** [δ 2.01 (9 H, s), 6.15 (2 H, s)] and **4c**. The intermediate decomposes more slowly ($t_{1/2} = 0.3$ h) into **3b** and acetamide. Some ($\sim 20\%$) of **4c** is also formed in this slower step.

The ^1H NMR and HPLC results assign k' to the disappearance of **1a-c** and k'' to the decomposition of **2a-c**. The data shown in Figure 2 are typical. At pH 1.97, the half-life of **1a** is calculated to be less than 0.5 s, so all the changes observable by HPLC (Figure 2A) must be attributed to the decomposition of **2a**. The HPLC peak of the intermediate decays away and peaks for the two products, **3a** and **4a**, appear in a first-order fashion on this

Table V. Observed and Predicted Yields of Hydrolysis Products for **1a-c**

conditions ^a	for 1a			
	% yields observed ^b		% yields predicted ^c	
	3a	4a	3a	4a
HCl, pH = 1.00	16 ± 1	83 ± 4	14.5	85.5
HCl, pH = 1.69	28 ± 1	72 ± 2	28.0	72.0
		(24.8 ± 1.5) ^d		
HCl, pH = 1.97	37 ± 2	63 ± 2	37.5	62.5
		(26.0 ± 1.3) ^d		
HCl, pH = 1.98	56 ± 1	46 ± 1	54.9	45.1
[KClO ₃] = 0.25 M		(15.7 ± 1.1) ^d		
HCl, pH = 2.30	47 ± 2	53 ± 2	49.7	50.3
		(24.7 ± 1.5) ^d		
HCl, pH = 3.04	67 ± 3	33 ± 2	68.4	31.6
		(23.9 ± 2.2) ^d		
acetate, pH = 3.83	72 ± 3	28 ± 1	74.0	26.0
acetate, pH = 4.62	76 ± 3	25 ± 1	75.1	24.9
acetate, pH = 5.70	78 ± 3	21 ± 2	76.7	23.3
phosphate, pH = 7.75 ^e	65 ± 5 ^f	1.3 ± 0.5	97.9	2.1
[KClO ₃] = 0.05 M				
borate, pH = 10.02 ^e	55 ± 5 ^f		100.0	0
[KClO ₃] = 0.05 M				

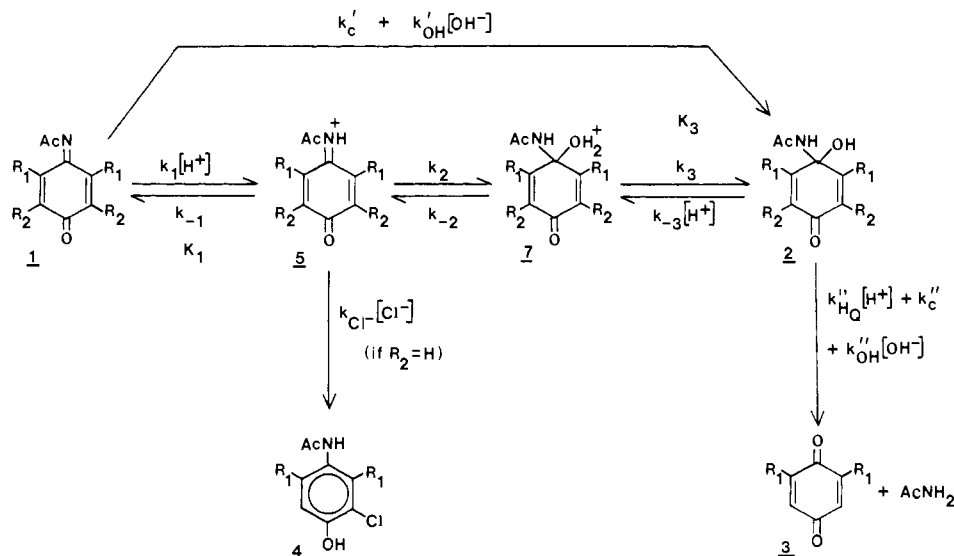
conditions ^a	for 1b :	
	% yield of 3b ^b	
HCl, pH = 2.29	100 ± 3	
HCl, pH = 3.05	102 ± 3	
acetate, pH = 3.76	98 ± 3	
acetate, pH = 4.65	102 ± 3	
acetate, pH = 5.61	105 ± 3	
phosphate, pH = 6.60	95 ± 3	
borate, pH = 9.17	87 ± 2 ^g	

conditions ^a	for 1c			
	% yields observed ^b		% yields predicted	
	3b	4c	3b	4c
HCl, pH = 0.31	86 ± 3	13.4 ± 0.5	86.0	14.0
		(10.1 ± 1.0) ^d		
HCl, pH = 1.01	91 ± 2	10.4 ± 1.1	89.7	10.3
HCl, pH = 2.01	92 ± 2	8.3 ± 0.7	91.5	8.5
acetate, pH = 4.61	99 ± 2	trace ^h	99.8	0.2
borate, pH = 9.58	95 ± 2 ⁱ		100.0	0

^a Total buffer concentration = 0.01 M, $\mu = 0.50$ M maintained with KCl or KCl-KClO₃. $T = 25.0 \pm 0.1^\circ\text{C}$. Initial concentration of **1** was ca. 1.0×10^{-4} M unless otherwise indicated. ^b Determined by HPLC analysis at completion of reaction. Limits of error determined from standard deviation of average of three injections. ^c Calculated from Scheme 1 and rate constants and ionization constants from Table VI as described in text. ^d Percent yield of **4** produced in the initial rapid phase (k') of the reaction. Determined from initial concentrations obtained by a least-squares fit of concentration vs time data to the first-order rate equation. ^e Initial concentration of **1a** = 2.5×10^{-6} M. ^f This is a lower limit since **3a** undergoes significant hydrolysis during the course of the hydrolysis of **1a** at this pH. The reduction product acetaminophen can also be detected in low yield ($<10\%$). ^g This is a lower limit since **3b** undergoes some hydrolysis during the course of the hydrolysis of **1b** at this pH. The reduction product 3,3-dimethylacetaminophen is present in low yield ($<2\%$). ^h $<0.5\%$. ⁱ This is a lower limit since **3b** undergoes some hydrolysis during the course of hydrolysis of **1c** at this pH.

time scale with rate constants that vary from 1.00×10^{-3} to $1.22 \times 10^{-3} \text{ s}^{-1}$. The value of k'' observed spectrophotometrically at this pH is $1.04 \pm 0.02 \times 10^{-3} \text{ s}^{-1}$. Note that although all of **3a**, within experimental error, is formed in this slow process, only about 60% of **4a** (from the intercept and infinity concentration of the calculated first-order curve) is formed in the k'' process. The rest of this product is formed in the more rapid (at this pH) k' process. The formation of **4a** in both phases of the reaction requires that the formation of **2a** be reversible. At $\text{pH} \geq 4.0$, all of **4a** appears to be formed in the k' process, so the reversion of **2a** to **1a** must be acid catalyzed only. At pH 0.31, k' is small enough that the disappearance of **1c** can be monitored (Figure 2B). The rapid appearance and slow decay of **2c** and the biphasic appearance of **3b** is also observed. Rate constants derived from the HPLC data are in good agreement with those determined spectrophotometrically. The appearance of **4c** (not shown) is also biphasic, but ca. 75% of it is formed in the first, more rapid (k') process. The data shown for **1b** at pH 6.55 in Figure 2C are typical of the

Scheme 1



situations in which **2** is not observable by spectrophotometric methods. The decay of **1b** and the appearance of **3b** are characteristically first-order and the observed rate constants are comparable to those obtained spectrophotometrically.

Yields of hydrolysis products obtained by HPLC are reported in Table V. Where it was possible to ascertain, the yields of **4a** or **4c** produced in the initial (k') phase of the reaction are reported along with their overall yields. These products are obtained only under acidic conditions, but **3a** and **3b** are major hydrolysis products under all pH conditions. The yields of **3a** and **3b** under alkaline conditions are less than quantitative in large part because of their hydrolyses. At pH 10.0, the hydrolysis rate constant of **3a** is $3.0 \times 10^{-4} \text{ s}^{-1}$. That calculated for **1a** from the kinetic data is $1.56 \times 10^{-3} \text{ s}^{-1}$, so a substantial fraction of **3a** (ca. 35%) had undergone hydrolysis by the time product analysis was performed ca. 1 h after initiation of the reaction. Since hydrolysis of **3b** is at least 10^2 -fold slower than that of **3a**, its hydrolysis reaction does not compete as effectively with its formation from **1b** and **1c** under alkaline conditions, and higher yields are observed in those two cases. Conjugate addition of OH^- to the 3-position of **1a** and **1c** was not observed and, based on detection limits, could account for no more than 1–2% of the hydrolysis under alkaline conditions.

Kinetic Simulations. The kinetic and product data for **1a** were analyzed in terms of the mechanism of Scheme I and the microscopic rate constants presented in Table VI. Detailed mechanisms for the breakdown of **2** to **3** by acid, neutral, and basic pathways and for the k'_c and k'_{OH} processes will be presented in the Discussion section. An explanation of the assignment of ionization constants and rate constants follows.

$\text{p}K_1$. The $\text{p}K_a$ of *N*-ethyl-*p*-benzoquinone imine is estimated to be 4.1 on the basis of the experimental values for the *N*-methyl and *N*-benzyl compounds of 3.70 and 2.85,¹⁹ and an assumed correlation of $\text{p}K_a$ with σ_1 of the substituent on the α -carbon. The (two-point) slope, ρ_1 , of -8.5 is similar to that observed for a variety of substituted methylammonium ions.²⁰ The inductive effect on the $\text{p}K_a$ brought about by substitution of a carbonyl for a methylene α to the N is -5.4 .^{21,22} The C–N rotational barrier provides an approximation to the resonance effect of the carbonyl group, since the rotational barrier is lost on protonation at N.^{22,23} The C–N rotational barrier calculated by MNDO for **1a** is 3.2 kcal/mol (see below), but MNDO typically underestimates this barrier by a factor of ca. 2.²⁴ A resonance effect of 6 kcal/mol decreases

Table VI. Microscopic Rate Constants and Ionization Constants Used in the Kinetic Simulations

constant ^a	estimated values ^b	
	1a	1c
$\text{p}K_1$	-5.7	
k_1	$1.2 \times 10^5 \text{ M}^{-1} \text{ s}^{-1}$	
k_{-1}	$6.0 \times 10^{10} \text{ s}^{-1}$ ^c	
k_2	$5.45 \times 10^7 \text{ s}^{-1}$	
k_{Cl^-}	$3.60 \times 10^7 \text{ M}^{-1} \text{ s}^{-1}$	
$k_1 k_2 / k_{-1}$	$1.09 \times 10^2 \text{ M}^{-1} \text{ s}^{-1}$	$1.42 \times 10^{-2} \text{ M}^{-1} \text{ s}^{-1}$
$k_{\text{Cl}^-} [\text{Cl}^-] / (k_1 + k_{\text{Cl}^-} [\text{Cl}^-])$ ^d	0.249	0.092
$k_{\text{H}_2\text{O}}''$	$7.04 \times 10^{-3} \text{ M}^{-1} \text{ s}^{-1}$	$3.54 \times 10^{-4} \text{ M}^{-1} \text{ s}^{-1}$
$\text{p}K_3$	-6.9	-5.9
k_3	$5.8 \times 10^{11} \text{ s}^{-1}$ ^e	$5.8 \times 10^{11} \text{ s}^{-1}$ ^e
k_{-3}	$7.3 \times 10^4 \text{ M}^{-1} \text{ s}^{-1}$	$7.3 \times 10^5 \text{ M}^{-1} \text{ s}^{-1}$
k_{-2}	$1.5 \times 10^6 \text{ s}^{-1}$	$1.44 \times 10^3 \text{ s}^{-1}$

^a Defined in Scheme I. ^b Estimated as described in the text. Other rate constants necessary for the kinetic simulation are given in Table IV. ^c See ref 26. ^d At $[\text{Cl}^-] = 0.5 \text{ M}$. ^e See ref 32.

$\text{p}K_1$ for **5a** by 4.4 units to -5.7 . The $\text{p}K_a$ of *N*-protonated amides of basic aliphatic amines has been estimated to be ca. -8 .^{22,25} Rotational barriers in these amides are typically 15–20 kcal/mol.²⁴ The precision of our value is estimated to be ± 2 largely because of the uncertainty in the estimate of the rotational barrier. Perrin has measured the deprotonation rate constant for *N*-protonated acrylamide,²⁶ and we take his value of $6.0 \times 10^{10} \text{ s}^{-1}$ for k_{-1} . This fixes k_1 at $1.2 \times 10^5 \text{ M}^{-1} \text{ s}^{-1}$.

k_2 and k_{Cl^-} . The lack of general-acid catalysis and the inverse isotope effect on $k_{\text{H}'}'$ indicate that proton transfer is not rate limiting, so to a good approximation, $k_{\text{H}'}'$ is given by eq 7. Then

$$k_{\text{H}'}' = \frac{k_1}{k_{-1}} (k_2 + k_{\text{Cl}^-} [\text{Cl}^-]) \quad (7)$$

$k_2 + k_{\text{Cl}^-} [\text{Cl}^-] = 7.25 \times 10^7 \text{ s}^{-1}$. Since **4a** accounts for $24.9 \pm 0.8\%$ of the products formed by the k' process in HCl solutions (see Table V), k_2 is $5.45 \times 10^7 \text{ s}^{-1}$ and k_{Cl^-} is $3.60 \times 10^7 \text{ M}^{-1} \text{ s}^{-1}$

(24) (a) Hoesterey, B.; Neely, W. C.; Worley, S. D. *Chem. Phys. Lett.* **1983**, *94*, 311–315. (b) Our own MNDO calculations on formamide and *N,N*-dimethyl formamide have yielded rotational barriers of 7.7 kcal mol⁻¹ and 5.5 kcal mol⁻¹, respectively. NMR measurements on formamide have yielded rotational barriers ranging from 16.8 to 21.3 kcal mol⁻¹, depending on the solvent: Sunners, B.; Piette, L. H.; Schneider, *Can. J. Chem.* **1960**, *38*, 681–688. Kamei, H. *Bull. Chem. Soc. Jpn.* **1968**, *41*, 2269–2273. Drakenberg, T.; Forsen, S. *J. Phys. Chem.* **1970**, *74*, 1–7. A recent gas-phase NMR measurement of the rotational barrier in *N,N*-dimethylformamide yielded ΔH^\ddagger of 19.7 kcal mol⁻¹: Ross, B. D.; True, N. S. *J. Am. Chem. Soc.* **1984**, *106*, 2451–2452.

(25) Kresge, A. J. *Acc. Chem. Res.* **1975**, *8*, 354–360.

(26) Perrin, C. L. *J. Am. Chem. Soc.* **1986**, *108*, 6807–6808.

(19) Fieser, L. *J. Am. Chem. Soc.* **1930**, *52*, 4915–4940.

(20) Fox, J. P.; Jencks, W. P. *J. Am. Chem. Soc.* **1974**, *96*, 1436–1449.

(21) Pracejus, H. *Chem. Ber.* **1959**, *92*, 988–998.

(22) Fersht, A. R. *J. Am. Chem. Soc.* **1971**, *93*, 3504–3515.

(23) Perrin, C. L.; Johnston, E. R. *J. Am. Chem. Soc.* **1981**, *103*, 4697–4703.

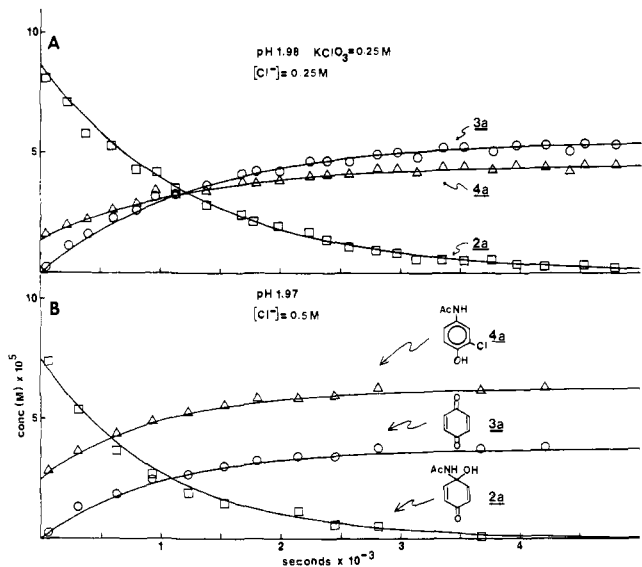
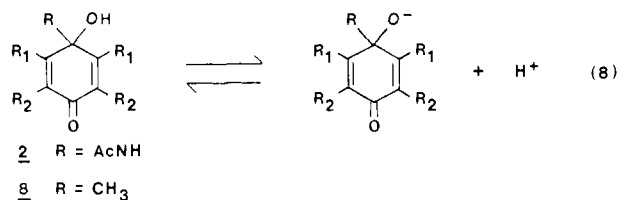


Figure 3. Comparison of the observed time dependence of **2a**, **3a**, and **4a** produced during the hydrolysis of **1a** with that predicted by Scheme I as a function of $[\text{Cl}^-]$. The theoretical lines were obtained from kinetic simulations using the data in Tables IV and VI: (A) pH 1.98, $[\text{Cl}^-] = 0.25 \text{ M}$, $\mu = 0.5 \text{ M}$; (B) pH 1.97, $[\text{Cl}^-] = 0.50 \text{ M}$, $\mu = 0.5 \text{ M}$.

($[\text{Cl}^-] = 0.5 \text{ M}$ in all these solutions).

$\text{p}K_3$. The $\text{p}K_a$ of **8a** is 13.05 ± 0.03 under our solvent and temperature conditions. If we assume $\rho_1 = -8.2 \pm 1.0$ for the substituent effect of R on the ionization equilibrium (eq 8)²⁰ then



the $\text{p}K_a$ of **2a** is 10.6 ± 0.3 based on standard values of σ_1 for CH₃ of -0.05 and AcNH of 0.25 .^{27,28} The $\text{p}K_a$ of **2a** is 4.9 units lower than that of MeOH.²⁹ If we assume the same substituent effect³⁰ on the deprotonation of the protonated alcohols, then the $\text{p}K_a$ of **7a** ($\text{p}K_3$) is -6.9 , based on the $\text{p}K_a$ of MeOH_2^+ of -1.98 at 25°C .³¹ The estimated error in $\text{p}K_3$ is ± 2 . We chose k_3 to be $5.8 \times 10^{11} \text{ s}^{-1}$, the rate constant for proton exchange between H_3O^+ and H_2O at 25°C .³² This fixes k_{-3} at $7.3 \times 10^4 \text{ M}^{-1} \text{ s}^{-1}$.

k_{-2} . Since proton transfers are not rate limiting in the acid-catalyzed formation of **4a** from **2a** (see below), k'' is given, to a good approximation, by eq 9,

$$k'' = k_c'' + k_{\text{OH}^-}''[\text{OH}^-] + k_{\text{H}^+}''[\text{H}^+] + \frac{k_{-3}[\text{H}^+]k_{-2}k_{\text{Cl}^-}[\text{Cl}^-]}{k_3(k_2 + k_{\text{Cl}^-}[\text{Cl}^-])} \quad (9)$$

where the last two terms correspond to the observed rate constant k_{H^+}'' . From the kinetic data for k'' (Table IV) and the product distributions for **3a** and **4a** produced in the same process (Table V), in the pH range 1.0–3.0, it is concluded that $87.7 \pm 3.8\%$ of k_{H^+}'' is given by the last term of eq 9 at $[\text{Cl}^-] = 0.5 \text{ M}$. This leads to a value of k_{H^+}'' of $7.04 \times 10^{-3} \text{ M}^{-1} \text{ s}^{-1}$ and k_{-2} of $1.5 \times 10^6 \text{ s}^{-1}$.

(27) Hansch, C.; Leo, A. *Substitution Constants for Correlation Analysis in Chemistry and Biology*; Wiley: New York, 1979; p 94.

(28) Charton, M. *J. Org. Chem.* **1964**, *29*, 1222–1227.

(29) Ballinger, P.; Long, F. A. *J. Am. Chem. Soc.* **1960**, *82*, 795–798.

(30) Funderburk, L. H.; Aldwin, L.; Jencks, W. P. *J. Am. Chem. Soc.* **1978**, *100*, 5444–5459.

(31) Bonvicini, P.; Levi, A.; Lucchini, V.; Modena, G.; Scorrano, G. *J. Am. Chem. Soc.* **1973**, *95*, 5960–5964.

(32) Luz, Z.; Meiboom, S. *J. Am. Chem. Soc.* **1964**, *86*, 4768–4769.

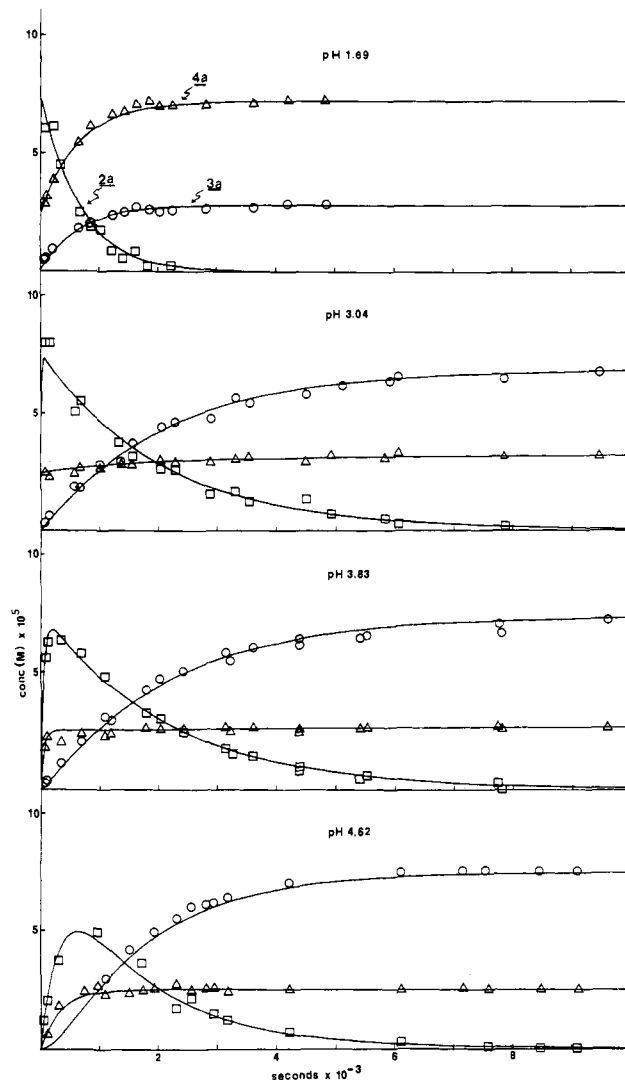


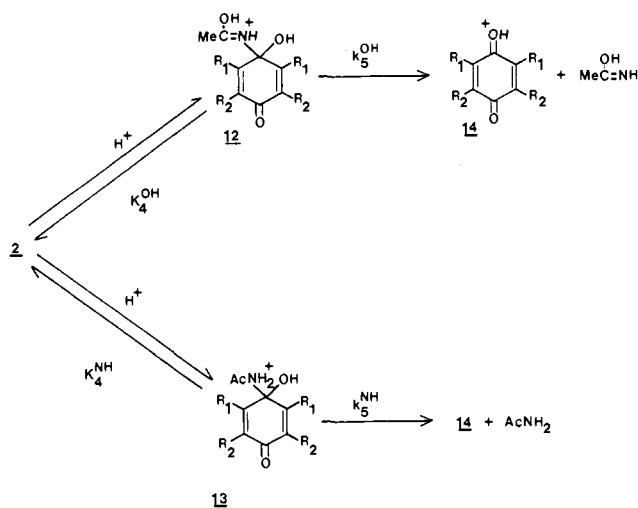
Figure 4. Comparison of the observed time dependence of **2a**, **3a**, and **4a** produced during the hydrolysis of **1a** with that predicted by Scheme I as a function of pH. The theoretical lines were obtained from kinetic simulations using the data in Tables IV and VI. Conditions: HCl solutions or 0.01 M HOAc–KOAc buffers, $\mu = 0.5 \text{ M}$ (KCl).

Kinetic simulations based on the rate constants in Tables IV and VI are shown in Figures 3 and 4. These show that the mechanism of Scheme I accurately predicts the time course of the hydrolysis of **1a**, its initial partitioning between **2a** and **4a**, and the variation of the partitioning of **2a** between the products **3a** and **4a** with $[\text{Cl}^-]$ and pH in the range 1.69 to 4.62. Predicted and observed product yields (Table V) are in very good agreement.

The individual rate constants of Scheme I are very dependent on $\text{p}K_1$ and $\text{p}K_3$, which are subject to considerable uncertainty. Most of the rate constants (except k_{-1} and k_{-3} , which are diffusion controlled) have an estimated precision of $\pm 10^2$. However, the overall equilibrium constant derived from the microscopic rate constants for the formation of **2a** from **1a** of 10.3 M^{-1} is independent of the $\text{p}K_a$ estimates ($[\text{H}_2\text{O}]$ is taken as 55.5 M). A value of 9.7 M^{-1} can be derived from the macroscopic constants k_{H^+}'' and k_{H^+}'' and the product distribution data of Table V, without reference to Scheme I. An equilibrium constant of this magnitude is consistent with our inability to detect **1a** by NMR in DCl solutions during the decay of **2a** into the final hydrolysis products.^{3a}

The kinetic and product data for **1c** were also analyzed in terms of Scheme I. No good model exists for the estimation of $\text{p}K_1$ for **5c**, but $\text{p}K_3$ of **7c** can be estimated as indicated above for **7a** from the $\text{p}K_a$ of **8c** of 14.1 ± 0.1 measured by titrimetric methods. The calculated value is -5.9 . Microscopic rate constants k_3 and k_{-3} were chosen as indicated for the unsubstituted case. From the

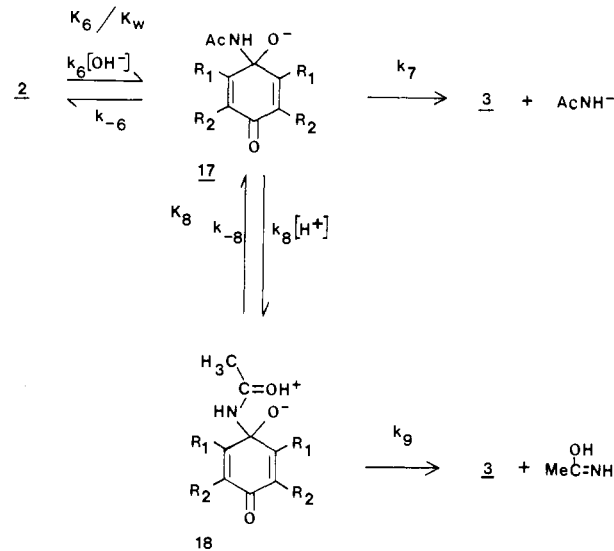
Scheme III



distant to expect a major effect on pK_a by solvation disruption. The electronic effects of the methyl substituents should be similar for both **5c** and **6c**. The charges on N and most other atoms including C-2 and C-6 are very similar in both structures according to MND0. In any case, the electronic effect of methyl substituents would increase pK_a , not lower it.

The tetrahedral intermediate **2** can be observed in all three cases under conditions in which k_H' governs the rate of disappearance of **1**. The disappearance of **2** is governed by specific-acid (k_H''), specific-base (k_{OH}''), and neutral (k_c'') pathways. Within experimental error, the neutral and basic pathways lead only to **3a** or **3b**, but the acid-catalyzed pathway for **2a** and **2c** produces significant amounts of **4a** and **4c** (see the Results Section). The acid-catalyzed rate constant for **2a** and **2c** also includes a significant component, k_{H_0}'' (Table VI), which produces **3a** or **3b**. The value of k_H'' in Table IV for **2b** is equivalent to k_{H_0}'' since the k_{Cl^-} path is not available to this compound. The generation of **4a** and **4c** under these conditions demonstrates the reversibility of the formation of **2a** and **2c** under acidic conditions, and this process must involve the same path (Scheme I) favored for the decomposition of **1**. The isotope effect data for **2b** indicate that the k_{H_0}'' process involves preequilibrium protonation at N or O (Scheme III) followed by rate-limiting loss of the amide. A correlation of pK_a of O-protonated acetanilides⁴³ vs pK_a of the corresponding anilinium ions gives a slope of 0.57 if substituents which interact with $-NH_2$ by resonance are excluded ($r = 0.988$). The ΔpK_a for protonated 4-amino-4-hydroxycyclohexa-2,5-dien-1-one (**15**) and methylammonium ion is assumed²⁰ to be the same as that for 4,4-dihydroxycyclohexa-2,5-dien-1-one (**16**) and methanol, which is calculated to be 4.9, the same as that for **2a** and methanol since σ_1 for OH and NHAc are equivalent.²⁸ Then pK_4^{OH} is -3.8 ± 2.0 based on the pK_a of O-protonated *N*-methylacetamide of -1.0 ,³⁸ the calculated ΔpK_a for **15** and methylammonium ion, and the factor of 0.57. An estimate for pK_4^{NH} of -10.7 can be obtained from Fersht's formulae for amides of basic aliphatic amines²² and the estimated pK_a for **15** of 5.7. The rate constants k_5^{OH} and k_5^{NH} would then be $4.4 \times 10^1 s^{-1}$ and $3.5 \times 10^8 s^{-1}$, respectively. The available data cannot discriminate between these two mechanisms. Although $pK_4^{OH} \gg pK_4^{NH}$, the initial leaving group in the O-protonation path is the imidic acid tautomer of acetamide which may be 7–12 kcal less stable than acetamide.^{22,37} Although tautomerization may occur simultaneously with expulsion of the leaving group, there will still be a considerably larger barrier to loss of the leaving group for the O-protonation path. The rather large substituent effects observed for k_{H_0}'' appear to reflect the relative stabilities of the protonated quinones **14a–c**. The methyl substituents of **14b** should stabilize the positive charge which is delocalized by a resonance interaction

Scheme IV



to the ring carbons bonded to the substituents. In **14c** the same steric hindrance to solvation discussed with respect to **5c** should occur. Apparently both of these factors are manifested in the transition state for this process.

The base-catalyzed and neutral decomposition of **2** can be discussed in terms of Scheme IV. The pseudo-first-order rate constant for the base-induced decomposition is then given by eq 10. Since $pK_6 = 10.6$ for **2a** (see the Results Section) and K_w

$$k_{OH}''[OH^-] = K_6 k_7 [OH^-] / K_w \quad (10)$$

$= 13.95$, k_7 is $2.0 \times 10^2 s^{-1}$. The rate constant for proton transfer to **17a** by H_2O (k_{-6}) is $4.5 \times 10^6 s^{-1}$ if the rate constant for proton transfer from **2a** to OH^- (k_6) is $10^{10} M^{-1} s^{-1}$,⁴⁴ so k_7 is small enough for the proton-transfer process to be in equilibrium. For **2b** and **2c**, pK_6 is 11.2 and 11.6, respectively (based on measured pK_a for **8b** and **8c** of 13.67 ± 0.08 and 14.1 ± 0.1 , respectively), and k_7 for **2b** and **2c** is then $1.0 \times 10^3 s^{-1}$ and $2.1 \times 10^3 s^{-1}$. The substituent effect observed in k_7 is consistent with the increasing driving force for expulsion of the leaving group provided by the increased basicity of the alkoxides in the series **17a–c**. The slope, β , of a plot of $\log k_7$ vs pK_6 is 1.0, which would be reasonable for a process with a very late (productlike) transition state. This is not unexpected for expulsion of the strongly basic $AcNH^-$.

The solvent isotope effect for this process (Table IV) is largely accounted for by the deprotonation equilibrium. For a number of alcohols and phenols with pK_a between 10 and 11 $\Delta pK_a(D_2O-H_2O) = 0.65 \pm 0.05$,³⁵ and $\Delta pK_w = 0.87$ in our solvent system, so the solvent isotope effect calculated for K_6/K_w is 0.60 ± 0.07 . This is essentially equivalent to the isotope effects observed for **2a** and **2b**. The isotope effect on k_{OH}'' for **2c** is lower, but there is considerable error associated with that number.

The rate constant k_c'' is given, according to Scheme IV, by eq 11 if a steady state in **17** and **18** is assumed. If $k_{-8} \gg k_9$ and $k_{-8}k_{-6}$

$$k_c'' = \frac{k_6 [OH^-] k_8 [H^+] k_9}{(k_9 + k_{-8}) k_{-6} + k_8 [H^+] k_9} \quad (11)$$

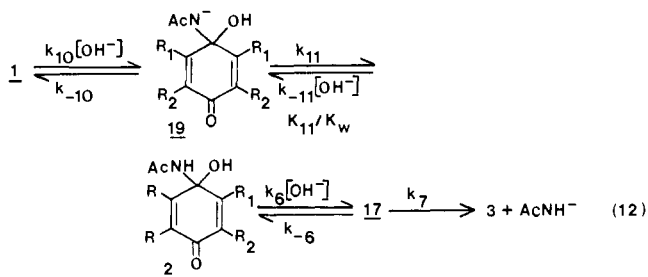
$\gg k_8 [H^+] k_9$, this reduces to the preequilibrium expression $K_6 k_9 / K_8$. An estimate of pK_8 is given by $pK_4^{OH} + 2.7$, which is -1.1 ± 2.0 for **18a**. The factor of 2.7 corrects for the effect of the negative charge on the pK_a of a zwitterionic carbinolamine (4.8)²⁰ moderated by the attenuation factor of 0.57 for substituent effects on the O-protonated amide. If k_8 is $10^{10} M^{-1} s^{-1}$,⁴⁴ then k_{-8} is $1.3 \times 10^{11} s^{-1}$. The observed value of k_c'' for **1a** (Table IV) and estimates of K_6 for **2a** and K_8 for **18a** require that $k_9 = 2.1 \times 10^8 s^{-1}$ for **18a**. The two assumptions required for the preequilibrium approximation to hold are valid at all $pH > 1.0$. The

(43) Giffney, C. J.; O'Connor, C. J. *J. Chem. Soc., Perkin Trans. 2* **1975**, 706–712.

(44) Eigen, M., *Angew. Chem., Int. Ed. Engl.* **1964**, *3*, 1–19.

small substituent effects observed for k_c'' may be due to partially compensating effects in K_6/K_8 and k_9 . The substituents will decrease K_6/K_8 since the ionization of **2** is more sensitive to the substituents than the ionization of **18** due to the attenuation of substituent effects in the O-protonated amide discussed above. The effect of substituents on k_9 should be similar to that discussed above for k_7 . The small observed isotope effects (Table IV) are in accord with expectations although fractionation factor data are incomplete.³⁹ Alternative pathways for the formation of **18** from **2**, including an intramolecular proton-switch process, the rate constant for which would have an upper limit in the thermodynamically favorable direction of ca. 10^8 s⁻¹,⁴⁵ do not appear to be kinetically viable.

Neutral and Basic Hydrolysis of 1. As in all the other cases no general catalysis is observed in the pH regions in which k_c' and k_{OH}' govern the rate of disappearance of **1**. The OH⁻-induced hydrolysis can be described by the mechanism of eq 12. The

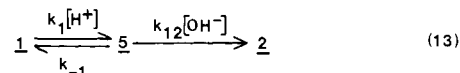


constants k_6 , k_{-6} , and k_7 were evaluated from the data for k_{OH}'' , and pK_{11} for **2a** can be estimated as 16.6 from the pK_a of *N*-methylacetamide (19.4),⁴⁶ ΔpK for MeOH and **16** (4.9), the assumption that substituent effects for deprotonation of OH and NH are equivalent,²⁰ and the attenuation factor of 0.57 described above. From a correlation of rate constants for base-induced amide N-H exchange vs pK_a of the amide for a series of peptides,⁴⁷ we estimate $k_{-11} = 1 \times 10^9$ M⁻¹ s⁻¹. This requires that $k_{11} = 4.5 \times 10^{11}$ s⁻¹, which is a reasonable value for a thermodynamically favorable proton transfer from solvent H₂O.^{32,44} The rate constant for decomposition of **19a** by this path is $k_{11}k_{OH}''/(k_{-11} + k_{OH}''')$ where k_{OH}''' is defined in eq 10. This yields a rate constant of 2.1×10^8 s⁻¹. Attack of OH⁻ on **2a** will be rate limiting unless $k_{-10} \geq 2.1 \times 10^8$ s⁻¹. This is not likely since the rate constant for expulsion of OH⁻ from deprotonated formaldehyde hydrate is only 3.9×10^2 s⁻¹.³⁰ The driving force for expulsion of OH⁻ from **19a** is larger than in deprotonated formaldehyde hydrate since $pK_{11} = 16.6$, while the pK_a (statistically corrected) of formaldehyde hydrate is 13.56,³⁰ but even if the rate constant for OH⁻ expulsion is directly proportional to pK_a , k_{-10} will only be ca. 4×10^5 s⁻¹. An alternative path involving an intramolecular proton switch to generate **17a** directly from **19a** would be competitive with the mechanism of eq 12 only if the proton switch in the thermodynamically favored direction proceeds with a rate constant $>10^9$ s⁻¹ (pK for the proton switch = $pK_6 - pK_{11} = -6.0$). Since the apparent upper limit for rate constants for intramolecular proton transfers between heteroatoms in a 1,3 relationship is ca. 10^7 s⁻¹,⁴⁸ it is not likely that this is the case.

The substituent effects on k_{OH}' (Table IV) are consistent with rate-limiting attack of OH⁻ on **1** (k_{10}). The ca. 4-fold difference in k_{OH}' for **1a** and **1c** is consistent with a modest steric effect for attack of OH⁻ on C-1, and the differences observed for **1b** and **1c** are consistent with previous observations that small unhindered

nucleophiles preferentially attack C-1 over C-4 in **3b**.¹² This selectivity was explained in terms of an electronic effect.¹² The isotope effects observed for k_{OH}'' (Table IV) are consistent with rate-limiting nucleophilic attack of OH⁻.^{35,39} The differences observed among the three compounds appear to be larger than experimental error, but it is unlikely that they reflect a change in rate-determining step.

The uncatalyzed reaction (k_c') is very slow and accounts for a significant part of the hydrolysis over a large pH range only for **1c** because of the depression in the k_H' term for that compound (Figure 1). Kinetic data (UV and HPLC) for **1c** show that the k_c' process does produce the intermediate **2c**. It is assumed that this also is the case for **1a** and **1b**. Attack of OH⁻ on **5**, eq 13,



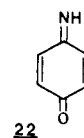
can be ruled out by the isotope effects as well as the magnitude of k_c' . The solvent isotope effect for the mechanism of eq 13 should be well below 1.0.^{35,39} The observed value for **1c** is 2.0; the others are slightly smaller, ca. 1.6 (Table IV), but this may be due to experimental error in determining k_c' for **1a** and **1b**. In any case, the observed effects are inconsistent with eq 13. The observed value of k_c' would require that $k_{12} > 10^{11}$ M⁻¹ s⁻¹ for $pK_1 < -1.7$. The estimated pK_1 of **5a** would require that k_{12} be $>10^3$ larger than the diffusion-controlled limit.⁴⁴

A concerted mechanism (**20**) is consistent with the isotope effects which suggest that proton transfer occurs in the rate-limiting step.^{35,39} The nature of the proton-transfer process is such

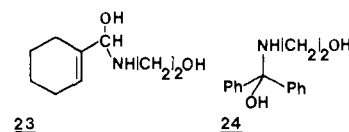


that it changes from very unfavorable to very favorable during the course of the reaction, so it can provide the driving force for the concerted process.⁴⁹ The concerted reaction avoids the formation of the very unstable zwitterionic species **21**.

Comparison with Imine Hydrolysis. The hydrolysis reactions of **1a-c** differ markedly from the hydrolysis of imines derived from aliphatic or aromatic amines,⁴ including *p*-benzoquinone imine (**22**),^{4f} in several respects. The carbinolamides **2a-c** can be readily



detected and even survive HPLC. The corresponding carbinolamines are rarely detected directly, although there is considerable evidence based on changes in rate-limiting step with pH or buffer concentration that they are intermediates in imine hydrolysis.⁴ They are not directly detectable because of the very low equilibrium constant for their formation from the corresponding imine. For example, K for the formation of **23** from the neutral imine



is estimated to be 1.4×10^{-7} M⁻¹ (assuming $[H_2O] = 55.5$ M),^{4c} while K for **24** can be estimated as 2.2×10^{-7} M⁻¹ from kinetic data^{4e} and pK_a estimates for the carbinolamine intermediates.⁵⁰ The corresponding equilibrium constants for **2a** and **2c** are 10.3

(45) Chang, K. C.; Grunwald, E. J. *Phys. Chem.* **1976**, *80*, 1422-1431. Maass, G.; Peters, F. *Angew. Chem., Int. Ed. Engl.* **1972**, *11*, 428-429. Bednar, R. A.; Jencks, W. P. *J. Am. Chem. Soc.* **1985**, *107*, 7135-7138.

(46) Molday, R. S.; Kallen, R. G. *J. Am. Chem. Soc.* **1972**, *94*, 6739-6745. The pK_a of *N*-methylacetamide quoted in this paper (17.7) was referenced to a pK_a of H₂O of 14.0, so 1.7 must be added to that value to obtain a pK_a useful in this work. See also ref 47.

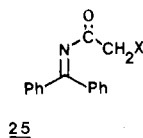
(47) Sheinblatt, M. *J. Am. Chem. Soc.* **1970**, *92*, 2505-2509. Sheinblatt, M.; Rahamin, Y. *J. Chem. Soc., Perkin Trans. 2* **1975**, 784-787.

(48) Luz, Z.; Meiboom, S. *J. Am. Chem. Soc.* **1963**, *85*, 3923-3925. Grunwald, E.; Fong, D.-W. *J. Am. Chem. Soc.* **1972**, *94*, 7371-7377.

(49) Jencks, W. P. *J. Am. Chem. Soc.* **1972**, *94*, 4731-4732.

(50) Sayer, J. M.; Jencks, W. P. *J. Am. Chem. Soc.* **1973**, *95*, 5637-5649.

and 0.14 M^{-1} , respectively (see the Results Section). The carbinolamide intermediates derived from benzophenone *N*-acylimines, **25**, are also readily observed during hydrolysis and have



an apparently large equilibrium constant for their formation.^{4d} The resonance stabilization of the amide group in the carbinolamide is apparently responsible for this. Our MNDO calculations indicate that the barriers to rotation about the C(O)-N bond in **1a** is significantly smaller than in simple amides. Since MNDO underestimates the rotational barrier in all amides, it is difficult to quantify the effect, but the differences in C(O)-N resonance interaction in **1a** and **2a** may contribute 5–10 kcal mol⁻¹ to $\delta\Delta G$. This would account for much of the difference in stabilities of carbinolamides and carbinolamines relative to their imine precursors.

Ordinary imines undergo nucleophilic attack by H₂O or OH⁻ exclusively through their conjugate acids at pH < 12.⁴ The *N*-acetylquinone imines **1a–c** undergo attack by both H₂O and OH⁻ in their neutral forms. At pH > 8 the k_{OH^-} path (Table IV, Figure 1) accounts for most of the rate of disappearance of **1a–c**. The pK_a s of most protonated imines are 2–4 units below that of the conjugate acid of the parent amine,⁴ so significant concentrations of the protonated imine exists throughout the pH region for most of these species. This is not the case for the much less basic **1a–c**. The rate constant for attack of OH⁻ on **5a** would have to exceed the diffusion-controlled limit by several orders of magnitude to account for the k_c' term of **1a**. Nucleophilic attack on neutral **1a–c** can compete because of the extremely low concentrations of **5a–c** available at pH > 7. The electron-withdrawing properties of the acetyl group also facilitate nucleophilic attack. Reaction of OH⁻ with a neutral imine would generate a species (the *N*-deprotonated carbinolamine) about 10²⁰ more basic than OH⁻. Although such a species would not have a finite lifetime in H₂O so that attack of OH⁻ would have to be simultaneous with proton transfer from H₂O or buffer acid to N, the example illustrates the difficulty of nucleophilic attack on neutral imines. Attack of OH⁻ on **1a** generates **19a**, which is not significantly more basic than OH⁻ ($pK_{11} = 16.6$ (eq 12)).

Decomposition of carbinolamines does not ordinarily occur via an anionic pathway because of the extremely poor leaving-group ability of the amine anion. Generally amine expulsion can occur only through the *N*-protonated or zwitterionic carbinolamine.^{4,5} For **1a–c**, the anionic pathway of Scheme IV is the dominant mode of decomposition of **2a–c** at pH > 5. Since the pK_a of AcNH₂ is 15.1,³⁸ AcNH⁻ is a much better leaving group than an ordinary amine anion.

Both the hydration and elimination steps of ordinary imine hydrolysis are usually subject to significant catalysis by buffers.^{4,5} No buffer effects are detectable in either step of the hydrolysis of **1b** at buffer concentrations of formic and acetic acid up to 0.20 M and at the lower concentrations (0.05 M) examined for **1a** and **1c**. Weak buffer catalysis (accelerations of 10 to 30% at 1.0 M buffer) was noted previously in the elimination step of the hydrolysis of **25**.^{4d} Effects of the same magnitude would have been observable at 0.2 M in our study. Buffer catalysis clearly amounts to less than 5% of the hydrolysis rates in this study. The isotope effects observed for H⁺ and OH⁻ catalyzed processes clearly indicate that these species are not behaving as general catalysts in the hydrolysis of **1a–c**. The predominant buffer catalysis observed in the hydration step for imines is general-base catalysis of the attack of H₂O on the protonated imine.^{4c,51} This is less important in **1a–c** because the protonated species **5a–c** are very reactive electrophiles with rate constants for uncatalyzed H₂O attack of ca. 10⁷–10⁸ s⁻¹. Corresponding rate constants for attack of H₂O on ordinary protonated imines are on the order of 10⁻⁴–10⁻¹ s⁻¹,⁴ so general base catalyzed attack of H₂O can provide a significant advantage. Although concerted general base catalyzed attack of H₂O on neutral **1a–c** or general-acid catalysis by proton donation to N with simultaneous attack of H₂O appear possible from the point of view of pK_a changes at reacting sites,⁴⁹ neither is important under the conditions we have examined to date.

Buffer catalysis of the dehydration step of imine hydrolysis involves general-base catalysis of deprotonation at OH of an *N*-protonated carbinolamine to form the zwitterionic carbinolamine by a simple rate-limiting proton transfer^{4c,5} or nonenforced catalysis by hydrogen bonding of the zwitterionic carbinolamine to the buffer acid.^{4d} Buffer catalysis by simple proton transfer cannot occur if the various ionized forms of the intermediate are already in equilibrium, which appears to be the case for **2a–c**. Nonenforced catalysis by H bonding is still a possibility. A search for weak buffer effects of the types indicated here will be commenced shortly.

Acknowledgment. This work is supported by a grant from the National Institutes of General Medical Sciences (Grant No. GM 38449-01). Support of the Faculty Research Council of Miami University is also acknowledged, as is the help of the Miami University Academic Computer Service, particularly Steve Moore, in installing and testing MOPAC 4.0 at Miami.

Supplementary Material Available: Tables I–III listing hydrolysis rate constants for **1a–c** and Table VII listing MNDO geometries for **1a**, **5a**, **6a**, **5c**, and **6c** (9 pages). Ordering information is given on any current masthead page.

(51) Funderburk, L. H.; Jencks, W. P. *J. Am. Chem. Soc.* **1978**, *100*, 6708–6714. Palmer, J. L.; Jencks, W. P. *J. Am. Chem. Soc.* **1980**, *102*, 6466–6481.